S. F. Baudic
Deepwater Systems Division,
ABB Lummus Global Inc.,
Houston, TX 77242-2833

A. N. Williams
Department of Civil and
Environmental Engineering,
University of Houston,
Houston, TX 77204-4791
e-mail: awilliams@uh.edu

A. Kareem
Department of Civil Engineering
and Geological Science,
University of Notre Dame,
Notre Dame, IN 46556-0767

A Two-Dimensional Numerical Wave Flume—Part 1: Nonlinear Wave Generation, Propagation, and Absorption

A numerical model is developed to simulate fully nonlinear transient waves in a semi-infinite, two-dimensional wave tank. A mixed Eulerian-Lagrangian formulation is adopted and a high-order boundary element method is used to solve for the fluid motion at each time step. Input wave characteristics are specified at the upstream boundary of the computational domain using an appropriate wave theory. At the downstream boundary, a damping region is used in conjunction with a radiation condition to prevent wave reflections back into the computational domain. The convergence characteristics of the numerical model are studied and the numerical results are validated through a comparison with previous published data. [DOI: 10.1115/1.1365117]

Introduction

The numerical wave tank concept has received considerable attention in the last few years; much effort has been directed towards developing the computational equivalent of a laboratory wave tank facility. Most of the work has been focused on developing fully nonlinear, inviscid time-domain solutions for wave generation and propagation in both two and three dimensions. Although a variety of different numerical techniques have been employed by the various investigators, the most popular, and successful, approach is undoubtedly the mixed Eulerian-Lagrangian (MEL) formulation originally developed by Longuet-Higgins and Cokelet [1]. In this approach, the wave propagation is treated as a transient process in which a time-stepping scheme is used to update the computational domain at successive instants during the simulation. The velocity potential at each instant of time is obtained through the application of the boundary integral equation method to the instantaneous fluid domain. This integral equation is solved in an Eulerian frame, while the time integration of the free-surface boundary conditions is performed in a Lagrangian manner. Several authors have extended the basic formulation of Longuet-Higgins and Cokelet to study the generation and propagation of nonlinear waves in a numerical wave-tank (NWT). Recent two-dimensional (flume) solutions include the works of Wang et al. [2,3], Clément [4], Skourup and Schaffer [5], and Grilli and Horillo [6,7]. Related perturbation-approach-based solutions for nonlinear wave generation in a two-dimensional wave flume have been developed in the frequency-domain by Hudspeth and Sulisz [8], Moubayed and Williams [9], and Schaffer [10], and in the time-domain by Zhang and Williams [11,12] and Stassen et al. [13]. In an NWT, the fluid motion is generated either by a prescribed wavemaker motion at the upstream boundary, or by specifying wave properties according to a chosen wave theory at the inflow boundary of the tank. In the fully nonlinear NWT approach (as opposed to a perturbation theory-based method), the second option is simpler, since it does not involve the constant updating of the fluid domain due to the wavemaker motion. This method is adopted in the present work.

In the NWT model, the computational fluid domain is truncated at a finite downstream boundary. A mechanism that prevents the waves that are propagating toward this boundary from being reflected back into the region in a nonphysical manner, is, therefore, an essential element in the simulation. The most common methods for accomplishing this goal are the use of a radiation condition, or active or passive wave absorbers. A radiation condition may be specified at infinity to make the wave propagation problem well posed. One approach for imposing Sommerfeld's radiation condition was first developed by Orlanski [14], in which the phase velocity required in this condition was evaluated numerically in the vicinity of the boundary. However, care must be taken to ensure that the computed phase velocity is relatively stable and non-negative. Passive wave absorption may be accomplished using a so-called damping layer or absorbing beach in front of the radiation boundary. In this approach, the free-surface boundary conditions inside the damping layer are modified by adding a dissipative term so that outgoing waves are absorbed with as little wave reflection as possible. This approach may be easily implemented; however, it requires that the computational domain be extended to accommodate the damping layer. Skourup [15] and Skourup and Schaffer [5] have devised an active wave absorption method for an NWT. The approach consists of implementing an active wavemaker at the outflow boundary of the flume whose movements are determined instantaneously from the time history of the local surface elevation in order to absorb the incident (outgoing) wave system. In the present work, an Orlanski-type radiation boundary condition will be specified; also, the performance of the radiation boundary condition when combined with a passive wave absorber (an absorbing beach) will be investigated.

Theoretical Development

A finite two-dimensional control domain, Ω, containing fluid is considered. A Cartesian coordinate system (x,z) is employed; the x-axis coincides with the reference position of the free-surface and the z-axis is directed vertically upward (see Fig. 1). The fluid is considered to be inviscid and incompressible, and the flow is assumed to be irrotational; therefore, it can be described in terms of a velocity potential $\phi(x,z,t)$ that satisfies Laplace's equation in the region of flow, namely

$$\nabla^2 \phi = 0 \qquad \text{in } \Omega \qquad (1)$$

On the free-surface, there are two boundary conditions, kinematic and dynamic. The kinematic boundary condition requires that no fluid be transported across the free-surface
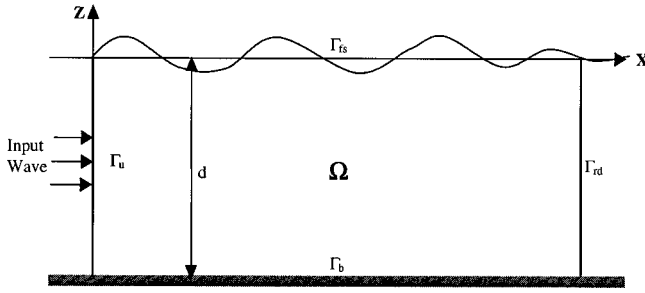
Fig. 1 Definition sketch

$$\frac{D\mathbf{x}_s}{Dt} = \nabla\phi \qquad \text{on } \Gamma_{fs} \qquad (2)$$

where $\mathbf{x}_s$ denotes the position vector of a free-surface particle. The dynamic boundary condition is based on the Bernoulli equation and is given by

$$\frac{D\phi}{Dt} = -g\,\eta + \frac{1}{2}(\nabla\phi\cdot\nabla\phi) \qquad \text{on } \Gamma_{fs} \qquad (3)$$

The tank bottom is a rigid and impermeable boundary; therefore

$$\frac{\partial\phi}{\partial n} = 0 \quad \text{on } \Gamma_b \qquad (4)$$

On the inflow boundary, Γ_u, the fluid motion is generated by imposing the properties (surface elevation, velocity potential, and/or normal velocity) of a known theoretical wave form (such as a single linear or nonlinear wave or multiple linear components). The input wave properties at the upstream wall are increased gradually using a ramping function, which initially satisfies a calm water condition and smoothly approaches unity as the simulation proceeds. The ramping function is given by

$$R_m = \begin{cases} \dfrac{1}{2}\left(1-\cos\left(\dfrac{\pi t}{T_m}\right)\right) & \text{if } t \le T_m \\ 1 & \text{if } t \ge T_m \end{cases} \qquad (5)$$

where T_m is specified as the length of time for which the input wave is ramped.

The computational domain is finite; therefore, on the outflow boundary, Γ_{rd}, a radiation condition is required. Physically, this condition ensures that the waves on this boundary are outgoing. In the present case, a Sommerfeld-type boundary condition is used. This condition takes the form

$$\frac{\partial\phi}{\partial n} = -\frac{1}{c}\frac{\partial\phi}{\partial t} \qquad \text{on } \Gamma_{rd} \qquad (6)$$

and requires the numerical evaluation of the phase velocity, c.

Finally, as the problem is solved in the time domain, the following initial conditions are also specified:

$$\left.\begin{aligned} \phi(x,z,0) &= 0 & (7a) \\ \eta(x,0) &= 0 \\ \nabla\phi(x,z,0) &= 0 \end{aligned}\right\} \text{in } \Omega \text{ and on all } \Gamma \qquad \begin{aligned} (7b) \\ (7c) \end{aligned}$$

The solution of the Laplace equation is based on a high-order boundary element method (HOBEM). The boundary element formulation is based on Green's second identity applied to the velocity potential ϕ and the free-space Green procedure leads to the following integral equation:

$$\alpha(\mathbf{x})\phi(\mathbf{x}) - \int_{\Gamma}\left\{\phi(\mathbf{x}_s,t)\frac{\partial G}{\partial n}(\mathbf{x},\mathbf{x}_s) - \frac{\partial\phi}{\partial n}(\mathbf{x}_s,t)G(\mathbf{x},\mathbf{x}_s)\right\}d\Gamma$$

$$= 0 \qquad (8)$$

where $\Gamma = \Gamma_{fs}\cup\Gamma_u\cup\Gamma_b\cup\Gamma_{rd}$; $\mathbf{x}_s = (x_s,z_s)$ is the position vector of an integration point which is situated at the boundary $\Gamma(t)$ of the domain; $\mathbf{x} = (x,z)$ is the position vector of the node under consideration; and $\alpha(\mathbf{x})$ depends on the position of $\mathbf{x}$ on the boundary.

In order to obtain a numerical solution to the BIE, a collocation method is used. The boundary $\Gamma(t)$ is discretized into M elements by using N collocation points. Within each element, a certain specified behavior of x, ϕ, and $\partial\phi/\partial n$ may be assumed. In the present case, cubic shape functions are introduced to describe the variation of the geometry and of the boundary functions over each four-node line element. The mapping relationship on a simple reference element is given by

$$S(\xi) = \sum_{q=1}^{4} N_q(\xi)S_q \qquad (9)$$

for $S = x$, z, ϕ, or $\partial\phi/\partial n$; N_q are the shape functions. The discretization method transforms the integral equation, Eq. (8), into a system of linear algebraic equations. Due to the high-order shape functions, the integrals involved in the equation cannot be evaluated analytically. Numerical integration over each boundary element is performed using Gauss-Legendre quadrature with 16 integration points.

The behavior of the discretized system at a corner node at the intersection of two sub-boundaries becomes a significant issue in cases where the formulation involves linear or higher-order boundary elements. In these cases, some collocation points are located at the intersection of two different domain sub-boundaries. Since the boundary conditions are, in general, different for each side of a corner point in the computational domain (e.g., on the input boundary and on the free-surface), a special approach is required to ensure continuity of the potential at these locations. A split-node technique has been developed by Grilli et al. [16] to allow specification of different boundary conditions at intersecting boundaries. Each corner node is represented by multiple nodes for which the coordinates of the nodes are identical, but their normal vectors are different. This technique has been used in the present numerical model to preserve the continuity of the potential ϕ and the compatibility of $\partial\phi/\partial n$ at the corner nodes.

After solving the boundary value problem and obtaining the fluid velocities and normal vectors on the free-surface, the free-surface boundary conditions given by Eqs. (2) and (3), considered as ordinary differential equations for ϕ and η, are advanced in time. For this purpose, a fourth-order Adams-Bashforth-Moulton (ABM4) scheme was used. The method is fourth-order but requires only two evaluations of the function $f(t,x,y,\phi)$ at each time step. An alternative would be to use the fourth-order Runge-Kutta (RK4) scheme that has a larger stability region [17], however, the ABM4 is generally preferred since the RK4 scheme requires twice as many function evaluations as the ABM4 method.

The simulation of nonlinear wave motions requires special attention to maintain numerical accuracy and avoid instability, while allowing the simulation to develop for longer times. In the MEL approach it is found that, as the simulation proceeds, the free-surface profile starts to develop sawtooth instabilities, due to the presence of higher wave modes [1]. In the present study, in order to remove these nonphysical oscillations, a five-point Chebyshev smoothing scheme is applied to the free-surface profile, the velocity potential and the normal velocity after a certain number of time steps. This smoothing method has been found to efficiently remove these nonphysical oscillations [18] and is applied every 5–20 time steps. In general, the smoothing interval must be reduced in the case of steeper waves. In each application considered herein, attention is given to maximizing the smoothing

interval for a given set of input parameters. Indeed, it is known that excessive smoothing may result in a significant reduction in the free-surface profile [19]. One possible source of these instabilities is use of a Lagrangian approach in the time-integration of the free-surface which results in high concentrations of collocation nodes in regions of high velocity [20]. Therefore, a regriding algorithm is also implemented during the simulation. A new, arclength-based free-surface mesh is generated each time the smoothing procedure is applied, and the velocity potentials and their derivatives at these new nodes are determined by interpolation.

Numerical Applications

To quantify the effect of the mesh size on the solution, three different meshes are used and their results compared. In each case a linear wave of known height, H_o, and period, T, is input at the upstream boundary to propagate downstream into the wave tank. First, a deepwater wave of height $H_o/h_o = 0.1$ and period $T/\sqrt{h_o/g} = 3.5515$ is considered. This case represents a relatively short wave with h_o/L corresponding to the linear deepwater limit, where L is the linear wavelength. Mesh sizes of $\Delta x = L/20$, $L/25$, and $L/30$ are considered, i.e., the number of nodes per wavelength, $N_w = 20$, 25, and 30. For all runs, a time step of $\Delta t = T/90$ is used. The wave elevation, velocity potential, normal derivative of potential and velocities on the boundary are smoothed every ten timesteps. The simulations were run for 21 wave periods. The wave data and tank dimensions are given in Table 1. For $N_w = 20$, the boundary was discretized into $M = 160$ cubic elements with a total number of $N = 484$ nodes, of which 234 were located on the free-surface. Similarly, for $N_w = 25$, there are $N = 610$ nodes and $M = 202$ cubic elements, and for $N_w = 30$, the corresponding values are $N = 724$ and $M = 240$. Figure 2 shows the wave profile at $x/h_o = 11$ for the different meshes. The figure indicates convergence of the surface elevation with mesh-size. An initial transient front can be seen, before the wave height stabilizes at a dimensionless time $t/\sqrt{h_o/g} \sim 70$. The steady state observed implies low reflection from the downstream boundary. It can be seen that an increased nodal density allows a more accurate computation of the wave kinematics, which, in turn, results in an

increase in the free-surface elevation. Similar results for the intermediate water depth wave of height $H_o/h_o = 0.3$ and $T/\sqrt{h_o/g} = 10.622$ (also described in Table 1), are shown in Fig. 3. To ensure the stability of the solution and allow a longer simulation time, a finer time step is required in this case. The mesh sizes tested are $N_w = 20$, 25, and 27, using a time step of $\Delta t = T/140$. Surface profiles are shown at a location $x/h_o = 55$ in the tank, and the simulations are carried out for 15 wave periods.

A convergence test with regard to the size of time step was also carried out. For the shorter wave, which has a steepness $kA_o = 0.157$, where $A_o = H_o/2$, three cases corresponding to time steps $\Delta t = T/70$, $T/90$, and $T/110$ were run with $N_w = 20$. The goal of these runs is to determine the maximum time step size (i.e., the minimum number of time steps per wave period) to obtain acceptable results. For the longer wave, where $kA_o = 0.092$, simulations were run for $\Delta t = T/120$, $T/140$, and $T/150$, again with $N_w = 20$. Time histories of the surface wave profile are shown in Figs. 4 and 5 for each case. It can be seen that the numerical results for the wave elevation do not differ as significantly with time step as they do for the different mesh sizes studied in the foregoing. It is concluded that the primary influence of the time step is on the stability of the simulation.

Fig. 3 Comparison of the dimensionless free-surface elevation at $x/h_o = 55$ due to a linear input wave of $kA_o = 0.094$, for various mesh sizes, calculated using $\Delta t = T/140$ and smoothing every 10 time steps

Table 1 Wave and numerical tank data

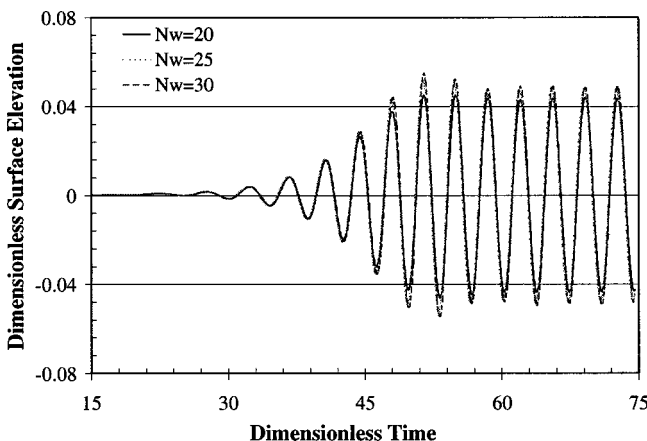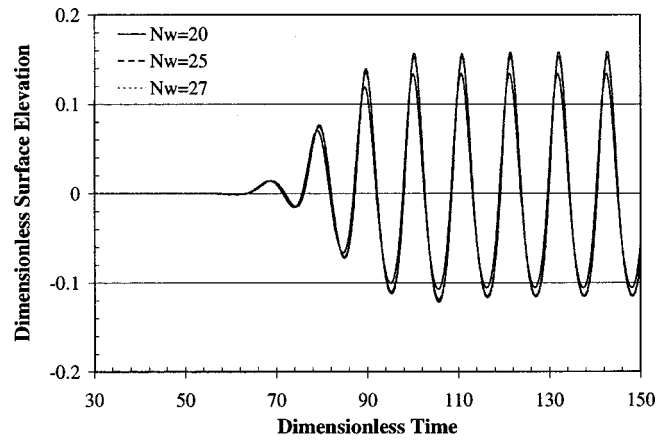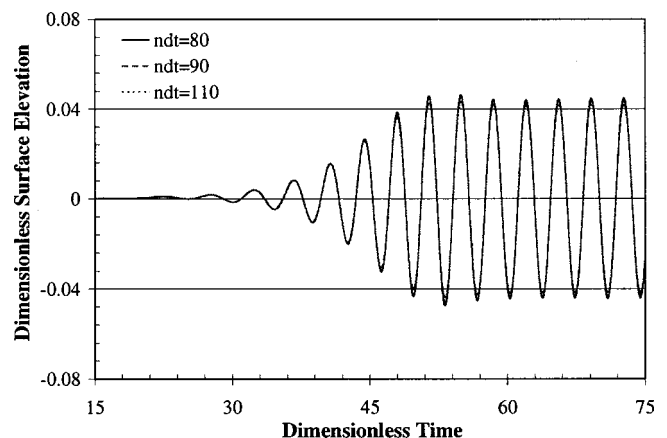| Wave no.	H_o/h_o	$T/\sqrt{h_o/g}$	L/h_o	kA_o	kh_o	l_d/h_o
1	0.1	3.5515	2.0324	0.1570	3.1415	24
2	0.2	10.622	10.261	0.0942	0.6283	120

Fig. 2 Comparison of the dimensionless free-surface elevation at $x/h_o = 11$ due to a linear input wave of $kA_o = 0.157$, for various mesh sizes, calculated using $\Delta t = T/90$ with smoothing every 10 time steps

Fig. 4 Comparison of the dimensionless free-surface elevation at $x/h_o = 11$ due to an input linear wave of $kA_o = 0.157$, for various time steps, calculated using $N_w = 20$ and smoothing every 10 time steps
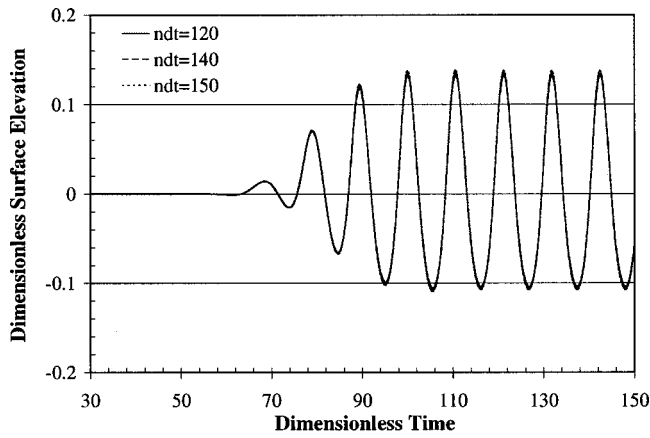
Fig. 5 Comparison of the dimensionless free-surface elevation at $x/h_o = 55$ due to an input linear wave of $kA_o = 0.094$, for various time steps, calculated using $N_w = 20$ and smoothing every 10 time steps
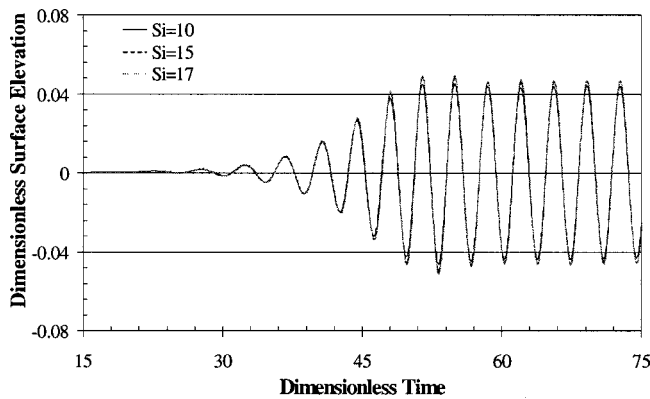
Fig. 6 Comparison of the dimensionless free-surface elevation at $x/h_o = 11$ due to an input linear wave of $kA_o = 0.157$, for various smoothing intervals, calculated using $\Delta t = T/90$ and $N_w = 20$

The influence of the smoothing interval on the computed free-surface profile has also been investigated. The free-surface profile for the short (i.e., steeper) wave case, corresponding to $kA_o = 0.157$, is shown at $x/h_o = 11$ for three different smoothing intervals in Fig. 6. It can be seen that the smoothing interval has some influence on the magnitude, but not the phase, of the generated waves: the larger the smoothing interval, the larger the wave height. For this data set, the computed wave heights obtained

when smoothing every 10 time steps are 6–7 percent smaller than those obtained when smoothing every 17 time steps. The difference in the computed wave heights between smoothing every 15 time steps to those when smoothing every 17 time steps is still on the order of 2 percent.

As stated previously, at the downstream boundary, a condition has to be specified in order to simulate outgoing waves, and thus avoid any reflection back into the computational domain. For this purpose, a Sommerfeld-Orlanski radiation condition has been adopted, Eq. (6). In the numerical implementation of this condition at timestep $(n+1)$, the "celerity" c is first determined based on the values of $\partial\phi/\partial t$ (obtained from the free-surface condition) and $\partial\phi/\partial x$ (obtained from the boundary integral equation), both at timestep n. If the calculated celerity is greater than $\Delta x/\Delta t$ it is set equal to $\Delta x/\Delta t$ for that time step, while if the calculated celerity is negative, then its value is set to zero for that timestep. A finite difference representation of the radiation boundary condition is applied at time step $(n+1)$ using this celerity to calculate the velocity potential $\phi(x,z,t_{n+1})$ on Γ_{rd}.

In the following, an energy absorption region is used in conjunction with the foregoing radiation condition. The energy absorption approach consists of adding an artificial dissipation term to the free-surface boundary conditions over the region of the free-surface adjacent to the radiation boundary. The purpose of this damping zone is to absorb the incident wave energy before it reaches the downstream wall and to further absorb any energy that is subsequently reflected back into the computational domain. The two free-surface boundary conditions, are modified as follows [21]:

$$\frac{D\mathbf{x}_s}{Dt} = \nabla\phi - \nu(x)(\mathbf{x} - \mathbf{x}_e) \quad (10a)$$

$$\frac{D\phi}{Dt} = -g\,\eta + \frac{1}{2}(\nabla\phi\cdot\nabla\phi) - \nu(x)(\phi - \phi_e) \quad (10b)$$

where the subscript e corresponds to the reference configuration for the fluid, that is, the initial conditions. In Eq. (10), $\nu(x)$ is a damping coefficient, assumed linear in wave frequency. It can be expressed as

$$\nu(x) = \alpha\omega\left(\frac{x - x_0}{L}\right)^2 \qquad fx \geq x_0, \quad x_0 = \beta L \quad (11a)$$

$$\nu(x) = 0 \quad \text{if} \quad x < x_0 \quad (11b)$$

where L is the wavelength, and α and β are constants. As in the case of real wave tank, numerical "beaches" are usually designed to attenuate the waves over a distance on the order of one wavelength. A comparison will be made of the efficiency of the absorbing beach, depending on the values of α and β chosen, i.e., the strength of the absorption and the length of the beach, respec-
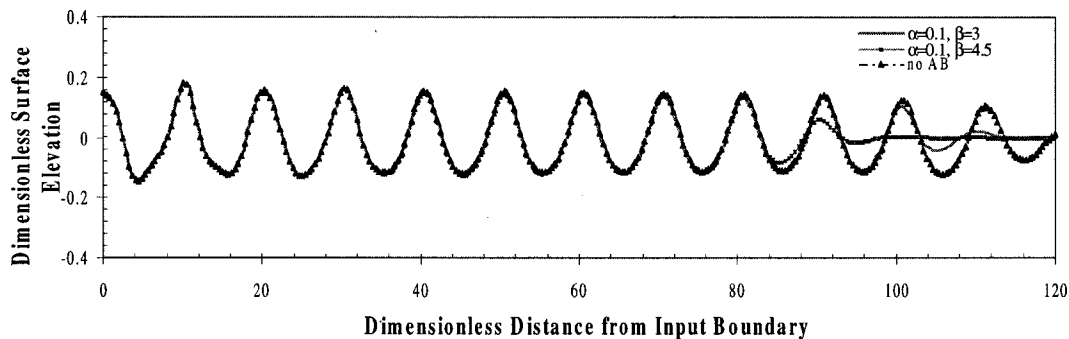
Fig. 7 Comparison of the dimensionless free-surface elevation at $t/T = 44.86$ due to an input linear wave of $kA_o = 0.094$, for various absorbing beach sizes, $\beta(L/h_o)$, and a constant α value, calculated using $N_w = 25$, $\Delta t = T/140$ and smoothing every 10 time steps
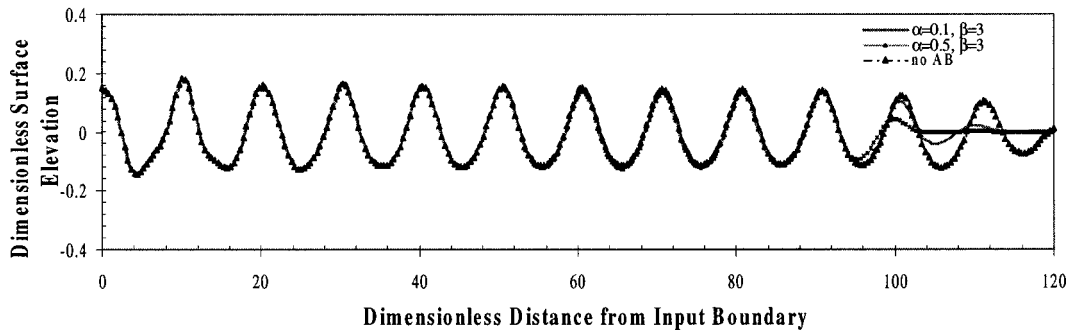
Fig. 8 Comparison of the dimensionless free-surface elevation at $t/T=44.86$ due to an input linear wave of $kA_o=0.094$, for various absorption strengths, α, with a constant β value, calculated using $N_w=25$, $\Delta t=T/140$ and smoothing every 10 times steps
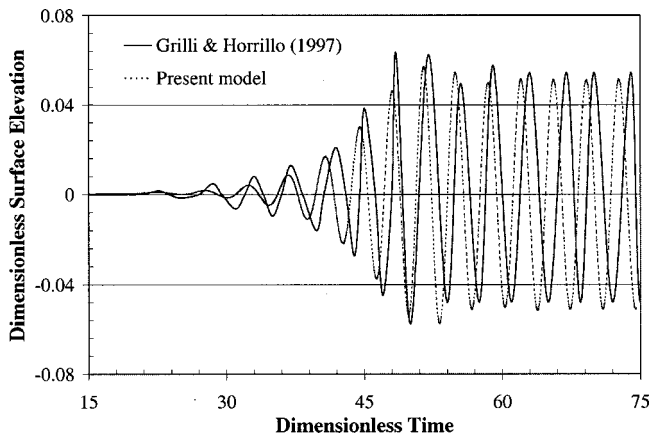
Fig. 9 Comparison of the results of the present model [6] for the dimensionless free-surface elevation at $x/h_o=11$ due to a Stokes fifth-order input wave of $kA_o=0.157$, calculated using $N_w=25$, $\Delta t=T/90$ and smoothing every 17 time steps

tively. If the absorption effect is too weak, a portion of the energy will be reflected from the downstream boundary; conversely, if the absorption effect is too strong, the damping zone will behave more like a solid boundary and wave reflection will again occur.

Results are only displayed for the case of long waves. Figure 7 presents the dimensionless free-surface profile at various dimensionless times for different values of the absorbing beach length, $\beta(L/h_o)$, and a fixed value of α. Similarly, Fig. 8 shows the dimensionless surface elevation at various dimensionless times for different values of α, and a constant value of β. It can be seen that use of a radiation condition alone gives satisfactory results, but better wave absorption is observed when using an absorbing beach. A substantial difference can be observed in the free-surface profiles when $\beta>1$. The wave amplitude decreases significantly when approaching the downstream wall; stronger absorption is also observed when $\alpha=0.5$.

Although the convergence study has shown satisfactory results, a comparison with previous authors verifies the accuracy of the model and thus completes the validation process. The present model has been compared with the fully nonlinear potential flow model developed by Grilli and Horrillo [6]. In their model, the boundary of the computational domain is discretized with quadratic isoparametric elements on the lateral and bottom boundaries, and mixed cubic elements on the free-surface. The incident wave was generated either by a numerical flap wavemaker or by stream function wave theory. They use an absorbing beach at the far end of the tank. A feedback procedure was developed to adaptively calibrate the beach absorption coefficient to absorb the

period-averaged energy of waves entering the absorbing beach. In some computations, they combined the beach model with an absorbing piston in order to achieve better absorption of low-frequency waves. A comparison between the free-surface obtained by the present approach and that of Grilli and Horrillo for the short wave case studied is shown in Fig. 9. It can be seen that the two sets of results are in reasonable agreement, with Grilli and Horrillo's model predicting slightly higher crests and flatter troughs. This is probably due to the differences in the input wave profiles and associated kinematics between the two models.

Conclusions

In the present paper, the simulation of fully nonlinear transient waves in a two-dimensional numerical wave tank was successfully completed. The time-domain analysis of the fully nonlinear wave motion was carried out using a mixed Eulerian-Lagrangian boundary element method. The Laplace equation was solved in a Eulerian frame using a boundary integral equation approach based on Green's second identity. The temporal updating of the free-surface was obtained from the fully nonlinear kinematic and dynamic free-surface boundary conditions by application of the fourth-order Adams-Bashforth-Moulton integration technique. The fluid boundary was discretized with four-node cubic line elements. A split-node technique was used to overcome the singularities and ensure continuity of the solution at the corner nodes. A radiation boundary condition was applied at the downstream boundary in order to simulate outgoing waves and avoid reflections back into the computational domain. Waves were generated at the inflow boundary by prescribing the surface elevation, velocity potential, and normal velocity according to an appropriate theoretical wave theory. A validation process was performed to demonstrate the accuracy and stability of the numerical model. A convergence study was carried out with respect to the parameters of mesh size, time increment, and smoothing interval. The influence of the theoretical form of the waves input into the numerical wave tank, and the efficiency of the radiation boundary condition have also been addressed. Finally, the robustness of the solution concerning the wave generation, propagation, and absorption problem was illustrated by a comparison with previous published results.

References

[1] Longuet-Higgins, M. S., and Cokelet, E. D., 1976, "The Deformation of Steep Surface Waves on Water—I: A Numerical Method of Computation," Proc. R. Soc. London, Ser. A, **350**, pp. 1–26.

[2] Wang, P., Yao, Y., and Tulin, M. P., 1994, ''Wave Group Evolution, Wave Deformation, and Breaking: Simulation using LONGTANK, a Numerical Wave Tank,'' Int. J. Offshore Polar Eng., **4**, pp. 200–205.

[3] Wang, P., Yao, Y., and Tulin, M. P., 1995, ''An Efficient Numerical Tank for Non-Linear Water Waves Based on the Multi-Subdomain Approach with BEM,'' Int. J. Numer. Methods Fluids, **20**, pp. 1315–1336.

[4] Clément, A. H., 1996, ''Coupling of Two Absorbing Boundary Conditions for 2D Time Domain Simulations of Free Surface Gravity Waves,'' J. Comput. Phys., **126**, pp. 139–151.

[5] Skourup, J., and Shaffer, H. A., 1997, ''Wave Generation and Active Absorption in a Numerical Wave Flume,'' *Proc., Seventh International Offshore and Polar Engineering Conference*, Honolulu, HI, **3**, pp. 85–91.

[6] Grilli, S. T., and Horrillo, J., 1997, ''Numerical Generation and Absorption of Fully Nonlinear Periodic Waves,'' J. Eng. Mech., **123**, pp. 1060–1069.

[7] Grilli, S. T., and Horrillo, J., 1998, ''Computation of Properties of Periodic Waves Shoaling Over Barred-Beaches in a Fully Nonlinear Numerical Wave Tank,'' *Proc., Eighth International Offshore and Polar Engineering Conference*, Montreal, Canada, 3, pp. 294–300.

[8] Hudspeth, R. T., and Sulisz, W., 1991, ''Stokes Drift in Two-Dimensional Wave Flumes,'' J. Fluid Mech., **230**, pp. 209–229.

[9] Moubayed, W. I., and Williams, A. N., 1994, ''Second-Order Bichromatic Waves Produced by a Generic Planar Wavemaker in a Two-Dimensional Wave Flume,'' Fluids and Structures, **8**, pp. 73–92.

[10] Schaffer, H. A., 1996, ''Second-Order Wave-Maker Theory for Irregular Waves,'' Ocean Eng., **23**, pp. 47–88.

[11] Zhang, S., and Williams, A. N., 1996, ''Time-Domain Simulation of the Generation and Propagation of Second-Order Stokes Waves in a Two-Dimensional Wave Flume Part I: Monochromatic Wavemaker Motions,'' Fluids and Structures, **10**, pp. 319–335.

[12] Zhang, S., and Williams, A. N., 1999, ''Simulation of Bichromatic Second-Order Stokes Waves in a Numerical Wave Flume,'' Int. J. Offshore Polar Eng., **9**, pp. 11–17.

[13] Stassen, Y., Le Boulluec, M., and Molin, B., 1998, ''A High-Order Boundary Element Model for 2D Wave Tank Simulation,'' *Proc., Eighth International Offshore and Polar Engineering Conference*, Montreal, Canada, **3**, pp. 348–355.

[14] Orlanski, I., 1976, ''A Simple Boundary for Unbounded Hyperbolic Flows,'' J. Comput. Phys., **21**, pp. 251–269.

[15] Skourup, J., 1996, ''Active Absorption in a Numerical Wave Tank,'' *Proc., Sixth International Offshore and Polar Engineering Conference*, Los Angeles, CA, **3**, pp. 31–38.

[16] Grilli, S. T., Skourup, J., and Svendsen, I. A., 1989, ''An Efficient Boundary-Element Method for Non-Linear Water Waves,'' Eng. Anal. Boundary Elem., **6**, pp. 97–107.

[17] Dommermuth, D. G., and Yue, D. K. P., 1987, ''Numerical Simulations of Nonlinear Axisymmetric Flows with a Free-Surface,'' J. Fluid Mech., **178**, pp. 195–219.

[18] Xu, H., 1992, ''Numerical Study of Fully Nonlinear Water Waves in Three Dimensions,'' Ph.D. dissertation, Department of Ocean Engineering, Massachusetts Institute of Technology, Cambridge, MA.

[19] Wu, G. X., and Eatock Taylor, R., 1994, ''Finite Element Analysis of Two-Dimensional Nonlinear Transient Water Waves,'' Appl. Ocean. Res., **16**, pp. 363–372.

[20] Kim, M. H., Celebi, M. S., and Kim, D. J., 1998, ''Fully Nonlinear Interactions of Waves with a Three-Dimensional Body in Uniform Currents,'' Appl. Ocean. Res., **20**, pp. 309–321.

[21] Cointe, R., 1989, ''Nonlinear Simulation of Transient Free-Surface Flows,'' *Proc., Fifth International Conference on Ship Hydrodynamics*, Hiroshima, Japan, pp. 239–250.